Hadronic b decays to open charm and a measurement of the CKM angle γ

V. V. Gligorov
On behalf of the LHCb collaboration
European Organization for Nuclear Research (CERN), Geneva, Switzerland

The LHCb detector is a general purpose forward spectrometer at the Large Hadron Collider, which exploits the $\approx$300 μb cross-section for $b\bar{b}$ production in 7 TeV proton-proton collisions to make precise measurements of b-hadron properties. The following results, all based on a 1 fb^{-1} data sample, are presented here : precision measurements of branching fractions and first observations of B meson decays to doubly charmed final states; searches for rare B meson decays to open charm final states; and a measurement of the CKM angle γ.

1 Introduction

The LHCb detector [1] at the Large Hadron Collider (LHC) is a single arm spectrometer optimized for the study of charm and beauty hadrons. The LHCb acceptance covers the pseudo-rapidity range $2 < \eta < 5$; in what follows "transverse" means transverse to the LHC beamline. The detector includes a high-precision tracking system, electromagnetic and hadronic calorimeters, two ring-imaging Cherenkov detectors for hadron identification, and muon chambers for muon identification. The combined tracking system has a momentum resolution $\Delta p/p$ that varies from 0.4% at 5 GeV/c to 0.6% at 100 GeV/c, an impact parameter [a] resolution of 20 μm for tracks with high transverse momentum, and a decay time resolution of 50 fs. Events are selected for further offline analysis by a trigger [2] system based around a multivariate [3] inclusive topological b-hadron selection.

The $\approx$ 300 μb cross-section [4] for $b\bar{b}$ production in 7 TeV proton-proton collisions, and a trigger system able to efficiently distinguish both leptonic and hadronic b-hadron decays from light-quark backgrounds, gives LHCb unprecedented statistical reach, particularly in the study of rare b-hadron decay processes. The results presented here are all based on 1 fb^{-1} of data collected in 2011, and concern b-hadron decays into "open charm" final states, those containing one or more charm (anti)quarks but not $c\bar{c}$ resonances. In the first half, precision measurements [5] of branching fractions and first observations of B meson decays to doubly charmed final states, as well as a search [6] for the rare $B_s \to D^{*-}\pi^+$ decay, are presented. In the second half, a combined measurement [7] of the Cabibbo-Kobayashi-Maskawa [9,10] (CKM) angle [b] γ based on measurements of decay rates and CP violation in $B^\pm \to D^0 K^\pm$ and $B^\pm \to D^0\pi^\pm$ decays is presented. Charge conjugation is implied throughout this document unless stated otherwise.

[a] Impact parameter is the transverse distance of closest approach between a track and a vertex, most commonly the primary proton-proton interaction vertex.

[b] The CKM matrix describes quark mixing in the Standard Model of particle physics. As it is a unitary, complex, matrix, relations between its elements can be depicted as a "unitarity" triangle in the complex plane. Testing whether the triangle closes and its angles (of which γ is one) add up to 180° therefore tests the unitarity of the matrix, and hence the Standard Model picture of quark mixing. For a compact review of the interest in measuring γ, see [8].

2 $B_{u,d,s} \to D_{u,d,s} D_{u,d,s}$ decays and a search for $B_s \to D^{*-}\pi^+$

Decays of B mesons into doubly charmed final states can be used to probe the CKM matrix elements, being sensitive to, for example, the $B^0_{d,s}$ mixing phases [11,12,13,14,15], the CKM angle γ [16,17], and the width splitting of the B_s states, $\Delta\Gamma_s$ [18,19]. This sensitivity is achieved through relating the observed branching fractions and CP asymmetries [c] to elements of the CKM mixing matrix. Different types of decay diagrams (tree-level, penguin, exchange, etc.) contribute to the various decays, and the relations between the experimental observables and the CKM parameters of interest to some extent rely on a knowledge of the relative size of these diagrams, as well as knowledge of rescattering contributions. It is therefore important to directly measure the branching fractions of these decays, in particular those which are primarily mediated by W-exchange such as $B_s \to D_{u,d} D_{u,d}$, where rescattering effects might substantially alter [20] a branching fraction estimate based on the CKM matrix elements. Similar arguments motivate a search for the rare decay $B_s \to D^{*-}\pi^+$, also assumed to be dominated by W-exchange.

The event selection is based in all cases on using the relatively long lifetime ($\approx$1.5 ps) and large mass ($\approx$5 GeV) of B mesons to distinguish them from light-quark backgrounds, and using particle identification (PID) information to isolate the signal decays from other, misidentified, b-hadron decays. Signal candidates must be selected by the multivariate B trigger algorithm, and to subsequently pass a multivariate preselection based on the more precise offline reconstruction.

In the $B \to DD$ modes, the D mesons are reconstructed in the Cabibbo-favoured modes $D^\pm \to K^\mp\pi^\pm\pi^\pm$, $D_s^\pm \to K^+K^-\pi^\pm$, $D^0 \to K^-\pi^+$, and $D^0 \to K^-\pi^+\pi^-\pi^+$. The D decay modes are distinguished from background based on PID information and by requiring that the D^0 canididate is well separated from the B decay vertex. The $D^\pm$ and $D_s^\pm$ decay modes can be backgrounds to each other : in this case, in addition to the requirements on PID and D vertex separation, candidates are reconstructed under both mass hypotheses and in the ambiguous cases strigent PID requirements are used to arbitrate between them. Multivariate selection are used to suppress light-quark background, trained on real data using abundant $B_{u,d,s} \to D_{u,d,s}\pi$ control modes, and taking into account kinematic correlations between the two charmed mesons in a $B \to DD$ decay. The reconstructed DD combinations are : $B_u \to D^0 D_s^\pm$, $B_{d,s} \to D^\pm D^\mp$, $B_{d,s} \to D^0\bar{D}^0$, $B_s \to D_s^\pm D_s^\mp$, and $B_{d,s} \to D^\pm D_s^\mp$.

In the search for $B_s \to D^{*-}\pi^+$, the selection is primarily concerned with the combinatorial background, as the $D^{*\pm} \to D^0\pi^\pm$ decay chain, with the very small $D^{*\pm} - D^0$ mass difference, makes the contribution from other, misidentified, B decays small. The selection is based on a neural network trained on the data itself, using the abundant $B^0 \to D^{*-}\pi^+$ control mode as a proxy for the signal and sidebands for the background. The training is performed with only a subset of the full sample used in the search, and the robustness of this method is verified by varying the size of the training sample.

Following the event selection, maximum likelihood fits are performed to the B mass distributions in order to extract the signal yields. Signal lineshapes are taken from simulated event samples, with the widths floated to account for different resolutions in data and simulation. In the $B \to DD$ case, backgrounds due to misidentified or partially reconstructed B meson decays are modelled based on simulated event samples, while the combinatorial background is parametarized by an exponential whose slope is taken from wrong-sign decays where possible and floated otherwise. In the $B_s \to D^{*-}\pi^+$ case, the combinatorial background is parametarized by a linear function with floating slope, while partially reconstructed B meson decays are parametarized by an exponential function with floating slope, and misidentified B meson decays are modelled using non-parametric lineshapes based on simulated events. An additional complication in the $B_s \to D^{*-}\pi^+$ case is the abundance of the $B^0 \to D^{*-}\pi^+$ control mode, the tails of whose mass distribution contaminate the $B_s \to D^{*-}\pi^+$ signal region due to resolution

[c] The CP asymmetries can be time-dependent, in the interference of mixing and decay, or time-integrated, in the decay itself, depending on the B meson and final state it decays into.

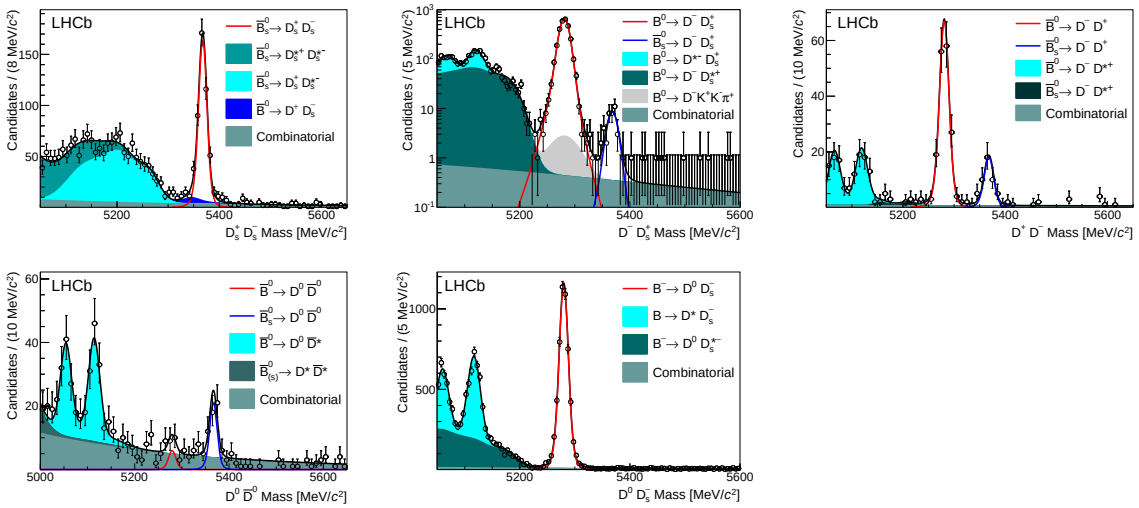

Figure 1: Fits to the B mass distributions : from left to right, $B_s \to D_s^{\pm} D_s^{\mp}$, $B_{d,s} \to D^{\pm} D_s^{\mp}$, $B_{d,s} \to D^{\pm} D^{\mp}$ (top row); $B_{d,s} \to D^0 \bar{D}^0$, $B_u \to D^0 D_s^{\pm}$ (bottom row). The fit components are indicated in the legends.

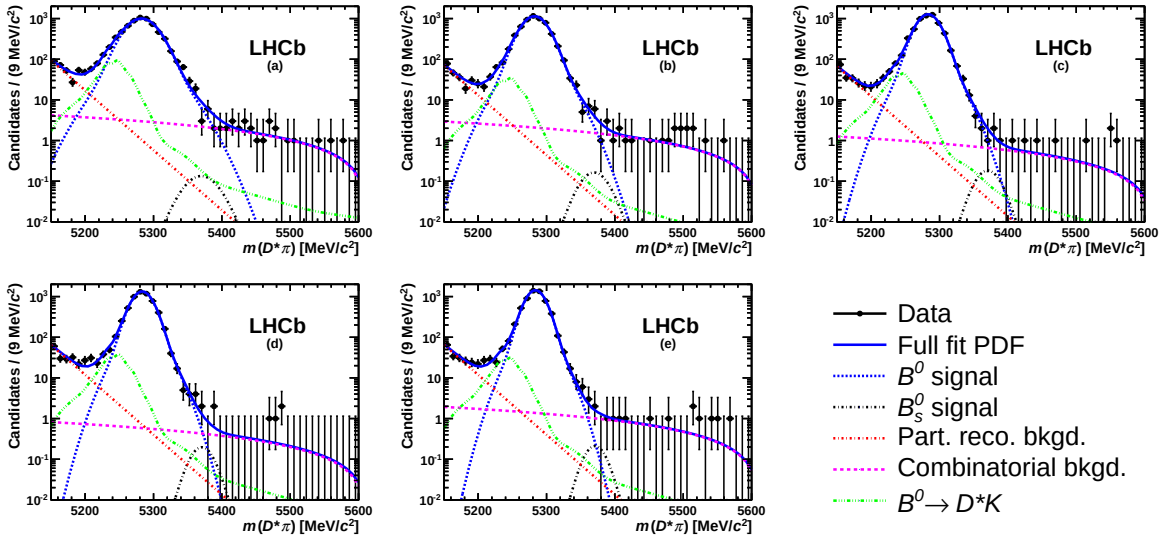

Figure 2: Fits to the B mass distribution in five bins of $\theta_{\rm bach}$. The components are indicated in the legend.

effects. The mass resolution, and hence the degree of contamination, depends on the opening angle ($\theta_{\rm bach}$) between the $D^{*\pm}$ and $\pi^{\pm}$ mesons, and the fit is performed simultaneously in five bins of this quantity, gaining around 20% in sensitivity compared to not binning in this quantity.

When determining whether a signal is significant or not, the fit is repeated with and without the signal component, with the signal lineshape fixed from simulation adjusted for known data-simulation differences. The likelihood ratio between these two fits is taken as a measure of the signal significance. In order to interpret observed signal yields as branching fractions, they are normalized to topologically similar decays whose branching fractions are known : $B_d \to D^{\pm} D^{\mp}$ is the normalization for $B_s \to D^{\pm} D^{\mp}$, $B_u \to D^0 D_s^{\pm}$ for $B_d \to D^0 \bar{D}^0$ and $B_s \to D^0 \bar{D}^0$, $B_d \to D^{\pm} D_s^{\mp}$ for $B_s \to D_s^{\pm} D_s^{\mp}$ and $B_s \to D^{\pm} D_s^{\mp}$, $B_d \to D^{\pm} D_s^{\mp}$ for $B_u \to D^0 D_s^{\pm}$, and $B_d \to D^{*-} \pi^+$ for $B_s \to D^{*-} \pi^+$. Efficiency differences between signal and normalization modes are taken from data control samples where possible and from simulation otherwise, while the ratio of the fragmentation fractions of B_s and B_d mesons are taken from the LHCb measurement [21].

The results of the fits are shown in Fig. 1 and 2. No signal is observed in the $B_s \to D^{*-} \pi^+$ decay, and an upper limit is set on the branching fraction $B(B_s \to D^{*-} \pi^+) < 6.1(7.8) \cdot 10^{-6}$ at the 90% (95%) confidence level using a Bayesian approach. In the $B \to DD$ decays, first

observations are made of the $B_s \to D^\pm D^\mp$, $B_s \to D^0\bar{D}^0$, and $B_s \to D^\pm D_s^\mp$ decays at 10.9, 10.7, and 10 standard deviations (σ) respectively. In addition there is a 2.95σ hint of the $B_d \to D^0\bar{D}^0$ decay. The measured ratios of branching fractions are

$$\begin{aligned}
\frac{\mathcal{B}(B_s \to D^\pm D^\mp)}{\mathcal{B}(B_d \to D^\pm D^\mp)} &= 1.08 \pm 0.20(\text{stat}) \pm 0.10(\text{syst}),\\
\frac{\mathcal{B}(B_s \to D^\pm D_s^\mp)}{\mathcal{B}(B_d \to D^\pm D_s^\mp)} &= 0.048 \pm 0.008(\text{stat}) \pm 0.004(\text{syst}),\\
\frac{\mathcal{B}(B_s \to D_s^\pm D_s^\mp)}{\mathcal{B}(B_d \to D^\pm D_s^\mp)} &= 0.55 \pm 0.03(\text{stat}) \pm 0.05(\text{syst}),\\
\frac{\mathcal{B}(B_s \to D^0\bar{D}^0)}{\mathcal{B}(B_u \to D^0 D_s^\pm)} &= 0.019 \pm 0.003(\text{stat}) \pm 0.002(\text{syst}),\\
\frac{\mathcal{B}(B_d \to D^0\bar{D}^0)}{\mathcal{B}(B_u \to D^0 D_s^\pm)} &= 0.0014 \pm 0.0006(\text{stat}) \pm 0.0002(\text{syst}),\\
&< 0.0024 \text{ at } 90\% \text{ CL}\\
\frac{\mathcal{B}(B_u \to D^0 D_s^\pm)}{\mathcal{B}(B_d \to D^\pm D_s^\mp)} &= 1.20 \pm 0.02(\text{stat}) \pm 0.06(\text{syst}).
\end{aligned}$$

The most significant source of systematic uncertainty is the knowledge of the fragmentation fraction ratio, while some uncertainty also arises from the limited samples of simulated events used for efficiency calculations and the unknown effective lifetime of some of the B_s CP eigenstates[d].

3 A measurement of the CKM angle γ from $B^\pm \to D^0 K^\pm$ decays

The CKM angle $\gamma = \arg\left[-V_{ud}V_{ub}^*/(V_{cd}V_{cb}^*)\right]$ is one of the least well measured parameters of the CKM matrix. One of the theoretically cleanest methods to access this weak phase is through measurements of γ-sensitive observables in $B^\pm \to D^0 K^\pm$ and $B^\pm \to D^0\pi^\pm$ decays [22]; as only tree-level diagrams contribute, such a measurement is insensitive to physics effects beyond the Standard Model and provides a reference for other measurements. The D^0 meson must be reconstructed in a final state that is accessible to both D^0 and $\bar{D}^0$ mesons, such that interference between the two amplitudes may give access to phase information. The observables are the charge and final-state separated decay rates, which can generally be written as

$$\Gamma(B^\pm \to D^0 K^\pm) \propto (r_D^2 + (r_B^K)^2 + 2r_B r_D \text{Re}(e^{i(\delta_B^K + \delta_D \pm \gamma)})), \quad (1)$$

where r_D is the ratio of the D^0 decay amplitudes, r_B is the ratio of the $B^\pm$ decay amplitudes, $\delta_{B,D}$ are the strong phases in the B and D decays.

Many different choices of final state are possible, and they must be combined in order to arrive at the best precision, not only because of the increased statistical sensitivity but equally because they have different associated systematic uncertainties. Three different LHCb analyses are combined, using the following types of D^0 decays :

- Two-body decays to K^+K^-,$\pi^+\pi^-$,$K^+\pi^-$, and $K^-\pi^+$. This is commonly referred to as the GLW/ADS analysis [22,23,24,25], and exploits information from both the $B^\pm \to D^0 K$ and $B^\pm \to D^0\pi^\pm$ decays in order to constrain γ. In the case of the D^0 decays to the singly Cabibbo-suppressed CP eigenstates (GLW), the signal yields are higher but the sensitivity

[d] Because of the non-negligible width difference in the B_s system, CP even and CP odd B_s decays have appreciably different lifetimes. This then affects their selection efficiency and hence the measured branching fractions, with the maximum variation found to be $\sim$3%.

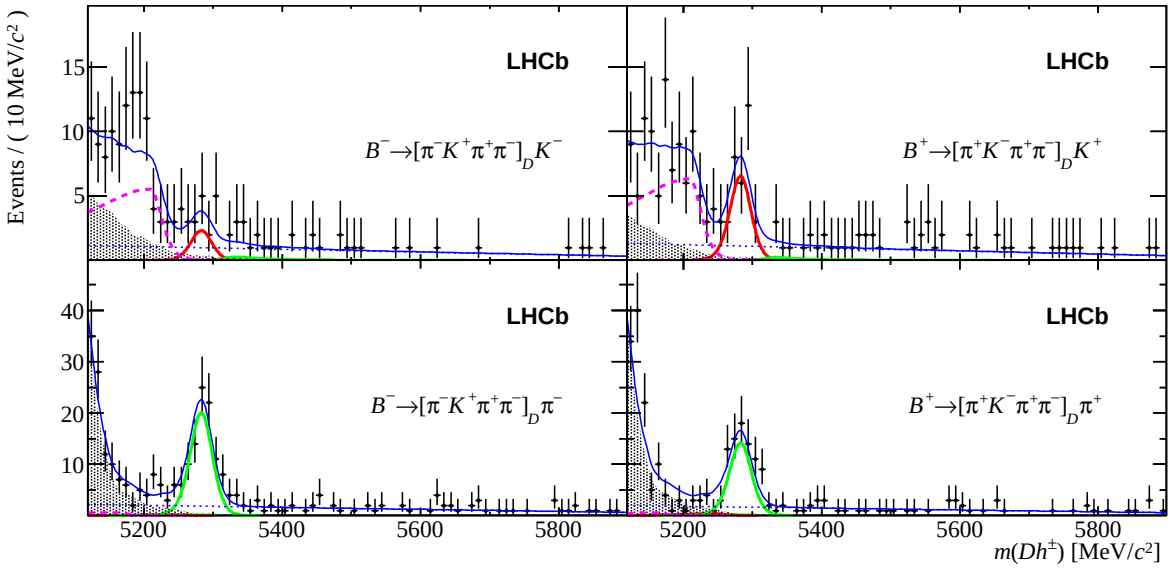

Figure 3: The $B^\pm \to D^0[K^\pm, \pi^\pm]$ signals for the doubly Cabibbo-suppressed four-body D^0 decay. The DK signals (top plots) are solid red, $D\pi$ signals (bottom plots) are solid green, background due to partially reconstructed $B^{\pm,0}$ decays is shaded, background due to partially reconstructed B_s^0 decays is dashed pink, and combinatorial backgrounds are dotted blue. The large CP asymmetry in the DK decays is visible by eye.

to γ is diluted because of the large relative size of the interfering B decay diagrams. This is mitigated in the ADS method by combining the favoured B decay with the doubly Cabibbo-suppressed D^0 decay, and the favoured D^0 decay with the suppressed B decay, leading to smaller yields but higher interference.

- Four-body decays to $K^+\pi^-\pi^+\pi^-$, and $K^-\pi^+\pi^+\pi^-$. This is analogous to the two-body ADS analysis, and exploits information from both the $B^\pm \to D^0 K$ and $B^\pm \to D^0\pi^\pm$ decays in order to constrain γ. The D^0 decay arrives to the four-body final state through a mixture of intermediate resonances, each decay path carrying its own amplitude and strong phase, however the analysis is a counting measurement which integrates over all these paths. This leads to a dilution in the sensitivity to γ, parametarized through a "coherence factor" which enters the decay rate equations.

- Three-body decays to $K^0_S\pi^+\pi^-$ and $K^0_S K^+ K^-$, which, like the four-body decays, proceed through a mixture of intermediate resonances. In this case, however, the information on the strong phases and amplitudes associated with each resonance is used in the analysis, leading to a greatly improved sensitivity to γ. This is commonly referred to as the GGSZ method [26], and can be thought of as a simultaneous ADS and GLW analysis due to the phase variation across the resonance(s) as you move through their peak.

The underlying measurements in all three contributing analyses are very much statistics limited, and that the dominant systematic uncertainties are related to control modes and are hence expected to scale with the statistical uncertainty. The observed (5.1σ) suppressed $B^\pm \to D^0[K^\pm, \pi^\pm]$ signals are shown in Fig. 3 for the four-body case in order to illustrate the cleanliness of the signals, achieved using multivariate selection techniques and LHCb's PID capabilities, even in the highest multiplicity final state.

The different measurements are combined using a frequentist technique, first for the $B^\pm \to D^0 K^\pm$ modes alone, and secondly for all the $B^\pm \to D^0[K^\pm, \pi^\pm]$ modes together. The $1-\mathrm{CL}$ contours for r_B^K and δ_B^K are presented for the $B^\pm \to D^0 K^\pm$ combination in Fig. 4, and the $1-\mathrm{CL}$ contour for γ is presented for both the $B^\pm \to D^0 K^\pm$ only combination and the full $B^\pm \to D^0[K^\pm, \pi^\pm]$ combination in Fig. 5. The fit results are presented in Tab. 1.

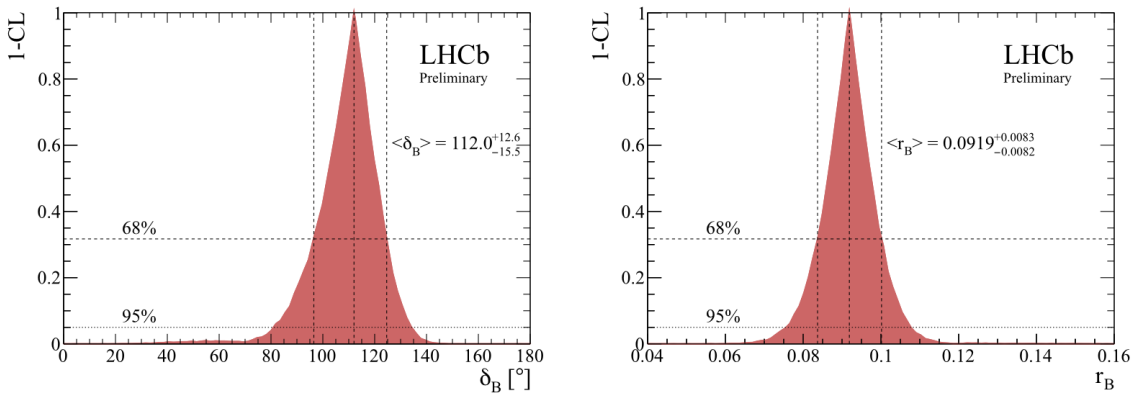

Figure 4: The $1-\mathrm{CL}$ contours for (left to right) r_B^K and δ_B^K for the $B^\pm \to D^0 K^\pm$ combination.

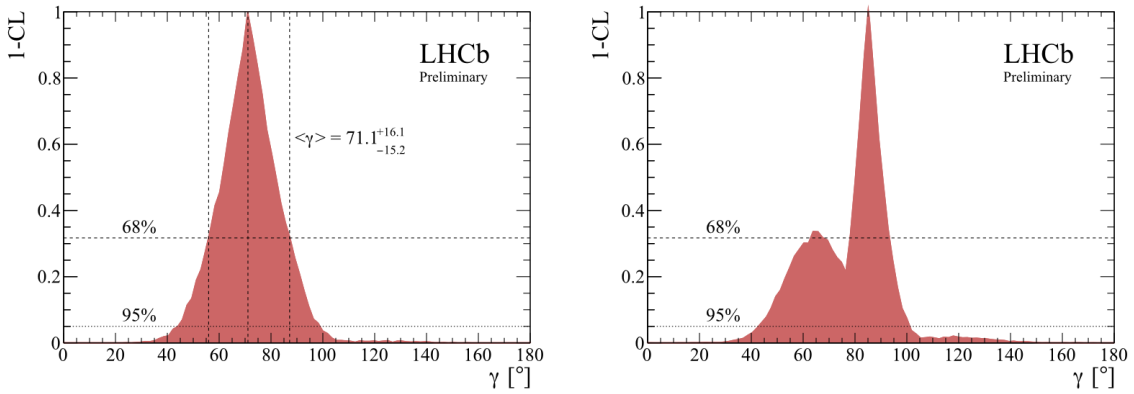

Figure 5: The $1-\mathrm{CL}$ γ contour for the (left) $B^\pm \to D^0 K^\pm$ and (right) $B^\pm \to D^0[K^\pm, \pi^\pm]$ combinations.

Table 1: Confidence intervals and central values for γ, r_B^K, δ_B^K for the $B^\pm \to D^0 K^\pm$ only (left) and for the $B^\pm \to D^0[K^\pm, \pi^\pm]$ combination (right). Central values are local likelihood maxima. All phases are modulo 180°.

Parameter	$B^\pm \to D^0 K^\pm$ only	$B^\pm \to D^0[K^\pm, \pi^\pm]$	
γ	$71.1°$	$63.7°$	$85.1°$
68% CL	$[55.4, 87.7]°$	$[61.8, 67.8]°$	$[77.9, 92.4]°$
95% CL	$[41.4, 101.3]°$	$[43.8, 101.5]°$	
r_B^K	0.919	0.0948	
68% CL	$[0.0837, 0.1002]$	$[0.0860, 0.1032]$	
95% CL	$[0.076, 0.108]$	$[0.078, 0.111]$	
δ_B^K	$112.0°$	$119.0°$	
68% CL	$[96.5, 124.6]°$	$[107.0, 129.1]°$	
95% CL	$[80.6, 134.3]°$	$[79.7, 137.9]°$	

4 Conclusion

The LHCb detector has operated successfully in 2011, collecting a 1 fb^{-1} data sample with an unprecedented statistical reach in the study of many B meson decays. In particular, it has been able to measure the CKM angle γ with a precision of $\sim 16^\circ$, which is comparable to the precision of the full dataset combinations of Belle [27] and BABAR [28]. With a further 2 fb^{-1} data sample, collected in 2012, on tape, even more precise measurements can be expected soon.

References

1. A. A. Alves *et al.* [LHCb Collaboration], *JINST* **3**, S08005 (2008).
2. R. Aaij *et al.* [LHCb Collaboration], arXiv 1211.3055, accepted in JINST.
3. V. V. Gligorov and M. Williams, *JINST* **8**, P02013 (2013).
4. R. Aaij *et al.* [LHCb Collaboration], *Phys. Lett.* B **694**, 209 (2010).
5. R. Aaij *et al.* [LHCb Collaboration], arXiv:1302.5854 [hep-ex].
6. R. Aaij *et al.* [LHCb Collaboration], arXiv:1302.6446 [hep-ex].
7. R. Aaij *et al.* [LHCb Collaboration], LHCb-CONF-2012-032.
8. J. Zupan, arXiv:1101.0134 [hep-ph].
9. N. Cabibbo, *Phys. Rev. Lett.* **10**, 531-533 (1963).
10. M. Kobayashi and T. Maskawa, *Prog.Theor.Phys.* **49**, 652-657 (1973).
11. R. Aleksan *et al.*, *Phys. Lett.* B **317**, 173-178 (1993).
12. A. I. Sanda and Z. Xing, *Phys. Rev.* D **56**, 341-347 (1997).
13. Z. Xing, *Phys. Lett.* B **443**, 365-372 (1998).
14. Z. Xing, *Phys. Rev.* D **61**, 014010 (2000).
15. X. Pham and Z. Xing, *Phys. Lett.* B **458**, 375-382 (1999).
16. A. Datta and D. London, *Phys. Lett.* B **584**, 81-88 (2004).
17. R. Fleischer, *Eur. Phys. J.* C **51**, 849-858 (2007).
18. K. De Bruyn *et al.*, *Phys. Rev.* D **86**, 014027 (2012).
19. R. Fleischer *et al.*, *Eur. Phys. J.* C **71**, 1789 (2011).
20. M. Gronau, D. London, J. Rosner, arXiv:1211.5785 [hep-ph].
21. R. Aaij *et al.* [LHCb Collaboration], arXiv:1301.5286 [hep-ex]
22. M. Gronau and D. Wyler, *Phys. Lett.* B **265**, 172-176 (1991).
23. M. Gronau and D. London, *Phys. Lett.* B **253**, 483-488 (1991).
24. D. Atwood, I. Dunietz, and A. Soni, *Phys. Rev. Lett.* **78**, 3257-3260 (1997).
25. D. Atwood, I. Dunietz, and A. Soni, *Phys. Rev.* D **63**, 036005 (2001).
26. A. Giri, Y. Grossman, A. Soffer, and J. Zupan, *Phys. Rev.* D **68**, 054018 (2003).
27. K. Trabelsi [BABAR Collaboration], arXiv:1301.2033 [hep-ex].
28. J. P. Lees *et al.* [BABAR Collaboration], *Phys. Rev.* D **87**, 052015 (2013).